

**Ab initio study of decohesion properties in oxide/metal systems**

J. I. Beltrán\*

*Université de Mons-Hainaut, Mons 7000, Belgium**and Instituto de Ciencia de Materiales de Madrid, CSIC, Madrid 28049, Spain*

M. C. Muñoz

*Instituto de Ciencia de Materiales de Madrid, CSIC, Madrid 28049, Spain*

(Received 12 June 2008; revised manuscript received 13 October 2008; published 18 December 2008)

Several studies of the decohesion properties of various oxide/metal systems have been performed recently by *ab initio* calculations. However, the use of different computational methods, which involve diverse approximations, energy functionals, or calculation conditions, makes the identification of general trends difficult. In the present work, a broad range of interfaces between an ionic oxide ( $\text{Al}_2\text{O}_3$ ,  $\text{ZrO}_2$ ,  $\text{HfO}_2$ , and  $\text{MgO}$ ) and a metal [either transition metal (TM) or Na], has been investigated systematically in order to find correlations among the work of separation ( $W_{\text{sep}}$ ) and the intrinsic properties of the interface, such as the crystal structure, the strain conditions, or the electronic properties of both constituents. Our main result is that the calculated  $W_{\text{sep}}$  adjusts very accurately to a parabolic dependence on the summed surface energies of the metal and the oxide, regardless of the oxide and metal components, crystal lattices, interface orientations, and atomic terminations. Furthermore,  $W_{\text{sep}}$  is mostly determined by the surface energies although for interfaces involving nonpolar oxide surfaces the contribution of the interfacial energy is not negligible. The strongest adhesion is found for interfaces formed by polar surfaces and bcc TM, e.g., the  $W_{\text{sep}}$  of  $\text{ZrO}_2(001)_\text{O}/\text{TM}$  interfaces changes almost by a factor of 2 depending on whether the TM has bcc or fcc structure. In addition, a correlation between the strain conditions of the equilibrium interface structure and the adhesion properties has been obtained. Finally, in order to predict metal/oxide systems whose mechanical properties are reinforced by the plastic deformation of the metal, we examine the expected behavior of the system beyond the elastic regime in the light of the calculated adherence at the interface. The comparison with the scarcely available experimental data provides good agreement for both the  $W_{\text{sep}}$  and the qualitative prediction of mechanical reinforcement.

DOI: [10.1103/PhysRevB.78.245417](https://doi.org/10.1103/PhysRevB.78.245417)

PACS number(s): 68.37.Nq, 68.55.-a, 71.20.Tx, 71.70.Ej

**I. INTRODUCTION**

Composite materials, constituted by oxides and metals, are of great importance for a wide range of technological applications such as: heterogeneous catalysis, multifunctional devices, fuel cells, or thermal barrier coatings.<sup>1,2</sup> Their technological interest arises from the possibility to obtain materials with tailored properties which may differ from those of their constituents. In addition, the combination of dissimilar materials may allow to better exploit the characteristics of both constituents.<sup>3</sup> The composite mechanical properties are determined by a complex balance among interactions both at the mesoscopic and atomistic level and in general they are intimately related to the formation of a good and strong metal/ceramic interface. For example, in cermet composites, metallic particles are embedded in a ceramic matrix in order to reinforce the composite mechanical properties by plastic deformation of the metal.<sup>4</sup> Such deformation provides a mechanism at the mesoscopic level, crack blunting, to reduce the energy of a propagating crack in the cermet. Even if there is a large lattice mismatch between the metal and the ceramic at the atomistic scale, reinforcement by crack blunting takes place in a few systems such as  $\text{Al}_2\text{O}_3/M$  ( $M=\text{Ni}$ ,  $\text{Cu}$ , and  $\text{Au}$ ) or  $\text{ZrO}_2/\text{Nb}$ .<sup>5,6</sup> However, for most ceramic/metal composites the reinforcement of the ceramic brittleness does not occur due to the failure of the system at the interface between the ceramic and the metal.<sup>7</sup> Therefore,

the mechanical properties of cermet materials are largely dependent on the metal/ceramic interface adhesion.

Atomistic theoretical studies of various oxide/metal systems, based on *ab initio* calculations, have been performed in order to describe at the atomic level the interactions at the interface<sup>8,9</sup> and to understand the origin of the experimental fracture energy data.<sup>10,11</sup> Nevertheless, most calculations refer to a specific system and for particular thickness and growth conditions. They are mainly focused on either isolated atoms<sup>12</sup> or single monolayers<sup>13</sup> of the  $\text{Al}_2\text{O}_3/\text{Ni}$  and  $\text{ZrO}_2/M$  ( $M=\text{Cu}$ ,  $\text{Pd}$ , and  $\text{Pt}$ ) systems,<sup>14</sup> making it difficult to achieve general trends for ceramic/metal interfaces. To our knowledge, the only systematic investigations were the studies of Bogicevic *et al.*<sup>15</sup> on the adsorption of metal overlayers on aluminum oxide, of Siegel *et al.*<sup>16</sup> on different ceramic/Al systems including  $\text{Al}_2\text{O}_3$ , carbides, and nitrides, and our previous studies on metal- $\text{ZrO}_2$  interfaces.<sup>6,7,17-19</sup> In the present work, we attempt to correlate the work of separation ( $W_{\text{sep}}$ )—the parameter characterizing the mechanical response of the composite—with the inherent properties of the metals and oxides forming the interface, extending the up to date results mainly focused on  $\alpha\text{-Al}_2\text{O}_3$ . Despite several approximations needed in order to investigate a wide range of systems, we are able to obtain general trends at the mesoscopic level which agree qualitatively with fracture energy measurements.

TABLE I. Lattice parameter (in Å), bulk modulus (in GPa), and cohesive energy (in eV) for the constituent metals of the ceramic/metal interfaces. Present results are compared with experiments and the experimental cohesive energy is obtained from Ref. 33. At the bottom of the table we can see the dispersion of our results with respect to the experimental measures.

System	Sym	$a/c$			$B_0$			$E_{\text{coh}}$	
		Present work	Expt.	Ref.	Present work	Expt.	Ref.	Present work	Expt.
Al	fcc	4.044	4.032	25	79	79	25	3.96	3.39
Rh	fcc	3.868	3.798	25	247	269	25	6.63	5.75
Cu	fcc	3.665	3.603	25	143	142	25	4.35	3.49
Ag	fcc	4.172	4.069	25	89	109	25	3.25	2.95
Ni	fcc	3.550	3.519	26	183	180	26	5.50	4.44
Pd	fcc	4.007	3.881	25	148	195	25	4.32	3.89
Pt	fcc	4.025	3.921	27	221	230	27	6.11	5.84
Mo	bcc	3.188	3.145	28	239	230	27	6.19	6.82
Na	bcc	4.201	4.225	25	6.2	7.5	25	1.01	1.11
Nb	bcc	3.315	3.250	27	136	170	27	6.28	7.57
Ta	bcc	3.324	3.300	29	197	200	27	8.48	8.10
W	bcc	3.197	3.160	29	285	310	27	8.28	8.90
Mg	hcp	3.230	3.210	30	34	35	30	1.56	1.51
		5.240	5.210						
Y	hcp	3.700	3.650	29	47	41	27	4.32	4.37
		5.850	5.730						
Zr	hcp	3.250	3.230	31	86	97	31	6.54	6.25
		5.210	5.150						
Hf	hcp	3.200	3.190	32	100	110	32	7.30	6.44
		5.050	5.040						
		$\sqrt{\frac{\sum(\frac{\text{theor-expt.}}{\text{expt.}})^2}{N}}$							
		1.016			0.880			1.130	

## II. THEORETICAL METHODOLOGY

The theoretical calculations have been performed with the *ab initio* SIESTA code<sup>20</sup> based on the density-functional theory (DFT),<sup>21,22</sup> using norm-conserving pseudopotentials and the generalized gradient approximation (GGA) in the Perdew-Burke-Ernzerhof scheme for the exchange and correlation term.<sup>23</sup> A linear combination of strictly localized numerical atomic orbitals constitutes the basis set. In our calculations the valence states for all transition metals (TMs) were described by double-zeta  $s$  and  $d$  shells and single-zeta  $p$  shell after polarizing the  $s$  shell.<sup>22</sup> The basis for oxygen and sodium comprised double-zeta  $s$  and  $p$  shells plus a single-zeta (polarized)  $d$  shell. Brillouin-zone (BZ) integrations were performed over a Monkhorst-Pack grid of the BZ of the primitive cell.<sup>24</sup> The mesh size depends on the material and is typically  $8 \times 8 \times 8$  for bulk metals,  $6 \times 6 \times 6$  for cubic oxides, and  $6 \times 6 \times 2$  for  $\alpha\text{-Al}_2\text{O}_3$ . For bulk calculations structural optimization was allowed until the residual forces in all the atoms were smaller than  $0.05 \text{ eV}/\text{\AA}$ . Tables I and II summarize the calculated equilibrium lattice parameter, bulk modulus, and crystal cohesive energy of the bulk metal and oxide phases, together with the experimental values. As expected from the GGA approximation, the calculated lattice parameters are slightly larger than the experimental values, with deviations below 2%, while the bulk moduli and cohe-

sive energies are reasonably well reproduced. Further, in the case of Ni we obtained a magnetic moment of  $0.6\mu_B$  in good agreement with previous calculations and experiments. For the oxides, the gap width is underestimated compared to the experimental values, a characteristic of DFT.

The interfaces have been modeled within a slab approach with periodic boundary conditions. The equilibrium structures were obtained relaxing both the cell size and the atomic positions until the forces in all the atoms were less than  $0.1 \text{ eV}/\text{\AA}$  and typically smaller than  $0.05 \text{ eV}/\text{\AA}$ . The supercell BZ was sampled using a Monkhorst-Pack tensor whose related in-plane  $K$ -grid cutoff is always larger than  $10.5 \text{\AA}$ , with no translation along the perpendicular interface vector. The cut-off value corresponds at least to the  $3 \times 4 \times 1$  Monkhorst-Pack tensor<sup>24</sup> for the largest interface real-space cell and typically takes the value of  $10 \times 10 \times 1$ . Details on the computational conditions and parameters can be found elsewhere.<sup>17-19</sup>

The initial configuration is formed by straining the metal to match the two-dimensional (2D) ceramic unit cell parallel to the interface. Therefore, only the metal is either compressed or stretched. The area strain parameter  $\Delta A_i$  is defined as the ratio of the (2D) unit-cell areas at the interface and at the ideal bulk termination for both ceramic ( $i=\text{CER}$ ) and metal ( $i=\text{MET}$ ). Thus, in the initial configuration  $\Delta A_{\text{CER}}=0$ . Relaxations, both in plane and perpendicular to the interface,

TABLE II. Same as Table I for the oxides forming the interfaces. Present results are compared to earlier calculations and experiments. Calculated cohesive energy is compared to the experimental formation enthalpy of the oxide from Refs. 33 and 54.

Oxides		$a$	$c$	$B_0$	$E_{\text{coh}}$ (eV)	Ref.
$\alpha$ -Al <sub>2</sub> O <sub>3</sub>	Present/GGA	4.85	13.16	213	15.27	
	PW/PW91	4.79	13.08	246		34
	PW/LDA	4.72	12.86	239		34
	OLCAO	4.83	12.61	242		35
	Expt.	4.76	13.00	253	17.37	36–38
MgO	Present/GGA	4.27		118	5.51	
	GGA	4.24		161		25
	GGA/PBE	4.28		140		39
	LDA	4.16		182		25
	GGA/ECP	4.27		151		40
	GGA/PAW	4.25		151		40
	Expt.	4.21		152	6.23	25 and 39
c-HfO <sub>2</sub>	Present/GGA	5.11		254	10.85	
	GGA	5.15		257		41
	GGA/PW91	5.00				42
	LDA	5.14		280		43
	LDA	5.09		289		41
	Expt.	5.08		280	11.52	42 and 44
c-ZrO <sub>2</sub>	Present/GGA	5.16		235	10.42	
	GGA/PW91	5.16				45
	LDA	5.08				45
	GGA	5.09				46
	LDA	5.04				47
	SC-TB	5.02				48
	HF	5.15				49
	Expt.	5.09		194–220	10.74	44 and 50–53

are allowed for the two components: the metal and the ceramic. In general, at the equilibrium configuration the ceramic material experiences some stress although almost all the lattice mismatch is adjusted at the metal side of the junction (see below). We allow relaxation of both constituents since composite materials usually show a granular structure where the lattice mismatch can be adsorbed by both the metal and the ceramic. In fact, cermets with large lattice mismatch between their constituents, as Al<sub>2</sub>O<sub>3</sub> and ZrO<sub>2</sub>/Nb, show atomic faceting with regions of abrupt interfaces at the atomic scale instead of planar sharp interfaces with a 2D unit cell corresponding to that of either the metal or the oxide.<sup>6</sup> Besides, surfaces of thin layers and nanoparticles of oxides may present structural parameters slightly different to those of the corresponding bulk crystals.<sup>7,55</sup>

We have performed two different kinds of calculations: the first corresponds to a supercell geometry including two slabs formed, respectively, by the metal and the ceramic, and the second model corresponds to the free overlayers of metals on top of the ceramic surface. In the former there are two identical interfaces in the supercell so it mainly describes interfaces between bulk systems as those present in cermets,

solid metal interfaces, composites, etc. In this case, the selected materials have always a 2D unit-cell area misfit smaller than 10%, except for two interfaces formed by Al<sub>2</sub>O<sub>3</sub> which compensate metal stretching with ceramic squeezing. A larger mismatch may lead to unphysical results since 10% area mismatch corresponds to 3%–4% differences of lattice parameters. It is expected that in this range of mismatch between ceramic and metal lattice parameters, the actual structures of the interfaces will present large coherent regions separated by misfit dislocations or small incommensurate disordered regions. In the second type of calculations, only performed for ZrO<sub>2</sub> and bcc metals, there is just one ceramic/metal interface and a free metal surface created by including a vacuum region large enough to inhibit interactions between the two terminating surfaces of the slab. Thus, this supercell geometry may model epitaxial metal film growths on ceramics as well as cermets with large lattice mismatch, which, as discussed above, may present faceted interfaces. Area mismatches up to 26%, which correspond to around 12% variation in the metal and oxide lattice parameters, have been considered. These calculations are performed in order to investigate the influence of the interface

adhesion properties on the enhancement of the fracture energy by the bridging mechanisms reported experimentally.<sup>6</sup> In that work, a clear correlation between the atomically matched interface facets and the observed mechanical enhancement mechanism in the composite materials has been established.

In order to quantify the adhesion properties with *ab initio* atomic simulations we have calculated the  $W_{\text{sep}}$ .  $W_{\text{sep}}$  is defined as the energy required to break interface bonds and thus is the reversible work needed to separate the interface into two free surfaces if the plastic and diffusional degrees of freedom are suppressed.<sup>17</sup> Two equivalent relations define the  $W_{\text{sep}}$ :

$$W_{\text{sep}} = (E_{\text{MET}} + E_{M_xO_y} - E_{\text{INT}})/(2A) = \sigma_{\text{MET}} + \sigma_{M_xO_y} - \gamma, \quad (1)$$

where  $E_{\text{MET}}$  and  $E_{M_xO_y}$  are, respectively, the total energy of the isolated relaxed metal and oxide  $M_xO_y$  systems,  $E_{\text{INT}}$  is the total energy of the complete metal/oxide structure, and  $A$  is the cross-sectional area.  $\sigma_{\text{MET}}$  and  $\sigma_{M_xO_y}$  denote metal and oxide surface energies, respectively, and  $\gamma$  is the interfacial energy. The calculated  $W_{\text{sep}}$  can be compared with the experimental decohesion contribution ( $\Gamma$ ) to the fracture energy, which characterizes the fracture properties of a brittle joint interface.<sup>4</sup>

Equation (1) shows that  $W_{\text{sep}}$  is also related to the interface  $\gamma$  and surface  $\sigma$  free energies, and therefore it can be analyzed in terms of the stability of the surfaces of both the metal and the oxide. To calculate the surfaces stabilities the procedure described in Refs. 17 and 56–59, which combines first-principles calculations with a thermodynamic approach, has been followed. There are two types of oxide slabs: stoichiometric (ST), with a number of atoms equal to an integer number of oxide formula units, and nonstoichiometric (NST) slabs. Surface and interface energies corresponding to NST interfaces can only be calculated as a function of the chemical potential of either the cation ( $\mu_M$ ) or the O ( $\mu_O$ ). Using the microcanonical ensemble,  $\gamma$  and  $\sigma$  are given as a function of  $\mu_O$  by

$$\begin{aligned} \mu_{M_xO_y} N_{M_xO_y} &= \frac{(N_M G_{M_xO_y}^{\text{bulk}})}{x} + \mu_O \left( N_O - \frac{N_{M_y}}{x} \right), \\ \gamma &= \frac{E_{\text{INT}} - \mu_{M_xO_y} N_{M_xO_y} - \mu_{\text{MET}} N_{\text{MET}}}{2A}, \\ \sigma &= \frac{(E_{M_xO_y} + E_{\text{MET}}) - \mu_{M_xO_y} N_{M_xO_y} - \mu_{\text{MET}} N_{\text{MET}}}{2A}. \end{aligned} \quad (2)$$

where  $x$  and  $y$  are the number of cation and O atoms per oxide formula unit, respectively,  $G_{M_xO_y}^{\text{bulk}}$  is the Gibbs free energy, and  $N_i$  is the number of atoms of type  $i$  ( $i = M, O, \text{MET}$ ). The allowed range of  $\mu_O$  is constrained by the chemical potential of the  $O_2$  molecule  $\mu_{O_2}^{\text{gas}}$  and the formation Gibbs free energy of the  $M_xO_y$  oxide,  $\Delta G_{M_xO_y}^f$ . Therefore,  $\mu_O$  fulfills the relation,<sup>17,58</sup>

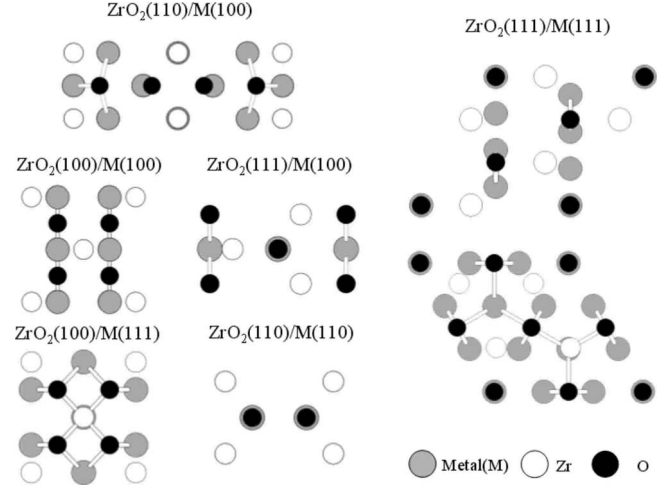


FIG. 1. Top view of the *c*-HfO<sub>2</sub>/metal or *c*-ZrO<sub>2</sub>/metal interfaces modeled for different metals and relative crystallographic orientations showing the metal-oxygen interface bonds. Only the Zr, O, and metal planes closer to the interfaces are represented. The relative crystal orientations of the ceramic and the metal are specified for each case.

$$\frac{1}{y} \Delta G_{M_xO_y}^f < \mu_O - \frac{1}{2} \mu_{O_2}^{\text{gas}} < 0.$$

Hereafter, the chemical potential will be given relative to the binding energy of molecular oxygen,  $\Delta \mu_O = \mu_O - \frac{1}{2} \mu_{O_2}^{\text{gas}}$ .

### III. INTERFACE GEOMETRY

We have performed a systematic study of the dependence of the adhesion properties on the choice of the metal at extended 2D interfaces. The selection of metals for each particular ceramic interface has been based on the value of the 2D lattice misfit. We have only considered low index surfaces with small commensurable unit cells and tried to analyze the influence of two effects: the lattice orientations, which imply changes in both structure and oxide polarity, and the metal electronic configuration. To this end, we have studied Na and transition metals with low and high occupancy of the *d* band, namely, Nb, Mo, Ta, and W on one side and Ni, Cu, Rh, Pd, Ag, and Pt on the other. It should be noted that a different bulk crystal structure corresponds to each group, bcc for Na and the TM of low *d*-band occupancy and fcc for the rest.

The unit cells used in our *c*-ZrO<sub>2</sub>/metal and *c*-HfO<sub>2</sub>/metal calculations appear in Fig. 1. All models correspond to fcc metals except the *c*-ZrO<sub>2</sub>(111)/metal(100) case (middle center in the Fig. 1), which refers to bcc metals. The unit cells corresponding to the interfaces formed by  $\alpha$ -Al<sub>2</sub>O<sub>3</sub> and MgO are represented in Fig. 2. For Al<sub>2</sub>O<sub>3</sub> the metals investigated are all bcc, while for MgO, Na is bcc and Ag fcc. The figure shows the unrelaxed configuration of our calculations where the strain induced by the misfit is assigned to the metal. For the oxide polar surfaces, where both metal and O terminations are possible, we focus the analysis on the O-ended cases although some metal terminations are

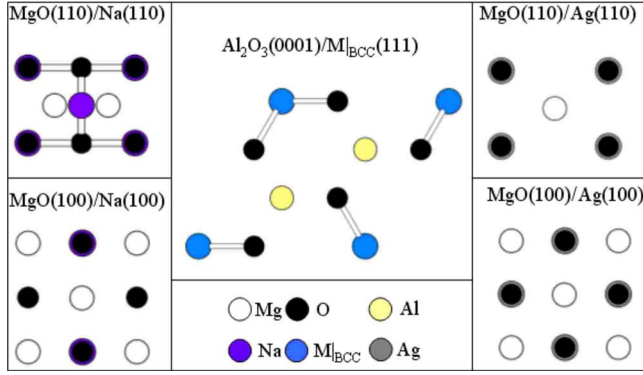


FIG. 2. (Color online) Same as Fig. 1 for the  $\text{Al}_2\text{O}_3(0001)_\text{O}/\text{metal}(111)$  and  $\text{MgO}/\text{metal}$  systems.

also investigated. All the interfaces are modeled by considering that interface reactions do not take place, and the adhesion properties are calculated under the elastic regime; so dissipative processes are not taken into account. Moreover, the calculations model ideal interfaces without defects as, for example, vacancies or interstitials.<sup>60</sup>

#### IV. WORK OF SEPARATION

A summary of our results for interfaces with less than 10% area misfit between constituents is shown both in Table

III for the NST interfaces and in Table IV for the ST slabs. Table V includes similar information for the interfaces with large mismatch (more than 10%). In the tables it is shown that the initial strain assigned to the metal is, after relaxation, distributed between both the metal and the oxide structures. Nevertheless, the final ceramic strain, which depends on the particular ceramic and crystal orientation, is usually smaller than that of the metal, never exceeds 5% (13%) and commonly corresponds to 2%–3% (5%–6%) for interfaces with nominal area mismatch of less (more) than 10%. In the tables, instead of the actual interface ceramic-metal bond, the ratio between the interface bond length and the sum of the respective ionic radii is shown. Note that for some interfaces there is a large dispersion of relative atomic positions within the 2D unit cell, as can be inferred from the large differences between the shortest metal-oxygen bond length (represented by  $\Delta d$ ) and the mean bond length ( $\langle \Delta d \rangle$ ). The disparity of the considered structures of ceramic and metals makes it difficult to establish trends among structures. Even for a given ceramic, i.e.,  $\text{ZrO}_2$ , there is a large variety of 2D interface unit cells, which differ in the number of metal-O bonds, in the metal to O coordination, and/or in the amount of strain. In addition, some interfaces involve Zr terminations or nonpolar  $\text{ZrO}_2$  surfaces and thus the metal-Zr interaction also contributes to the adhesion.

Even though a set of general common properties can be sketched for the interfaces studied, some of them are not

TABLE III. We show for the interfaces with less than 10% mismatch and constituted by a NST ceramic slab: the out-of plane orientation of both constituents, the ratio between the shortest bond length between the metal and the ceramic (either with an anion or cation), and the sum of the ionic radii of the atoms forming the bond ( $\Delta d$ ), and the same ratio taking the mean bond length instead of the shortest one ( $\langle \Delta d \rangle$ ); the difference between the average interface Mulliken charge and the bulk charge ( $\Delta Q$ ) for the ceramic and metal atoms at the interface; the ratio of the 2D unit-cell areas at the interface and at the ideal bulk termination ( $\Delta A$ ) for both ceramic and metal; and the work of separation ( $W_{\text{sep}}$ , in  $\text{J}/\text{m}^2$ ).

NST ceramic	$\Delta d$	$\langle \Delta d \rangle$	$\Delta Q_{\text{CER}}$	$\Delta Q_{\text{MET}}$	$\Delta A_{\text{CER}}$	$\Delta A_{\text{MET}}$	$W_{\text{sep}}$
$\text{Al}_2\text{O}_3(0001)_\text{O}/$							
Ta(111)	0.99	1.03	-0.02	-0.77	1.00	1.07	10.47
W(111)	1.04	1.06	-0.05	-0.57	0.97	1.12	9.76
Mo(111)	1.02	1.04	-0.09	-0.45	0.97	1.12	9.58
Nb(111)	1.02	1.06	-0.08	-0.65	1.02	1.09	9.26
$\text{ZrO}_2(100)_\text{O}/$							
Ni(100)	0.92	0.92	-0.16	-0.28	1.01	1.06	5.74
Cu(100)	0.97	0.97	-0.17	-0.27	1.02	1.01	5.08
Rh(111)	0.89	0.89	-0.17	-0.22	1.01	1.03	4.02
Pt(111)	0.90	0.92	-0.21	-0.30	1.05	1.00	3.37
$\text{ZrO}_2(100)_\text{Zr}/$							
Ni(100)	1.05	1.05	0.42	0.19	0.99	1.05	5.01
Cu(100)	1.10	1.10	0.57	0.10	1.02	1.01	3.66
$\text{HfO}_2/\text{Ni}(100)$							
$\text{HfO}_2(100)_\text{O}$	0.92	0.93	-0.14	-0.25	1.01	1.04	6.26
$\text{HfO}_2(100)_\text{Hf}$	1.03	1.03	0.34	0.24	0.99	1.02	5.54

TABLE IV. Same as Table III for interfaces constituted by ST ceramics.

ST ceramic	$\Delta d$	$\langle \Delta d \rangle$	$\Delta Q_{\text{CER}}$	$\Delta Q_{\text{MET}}$	$\Delta A_{\text{CER}}$	$\Delta A_{\text{MET}}$	Wsep
<b>ZrO<sub>2</sub>(111)<sub>O</sub>/</b>							
Ta(100)	0.99	1.01	-0.03	-0.21	0.95	0.99	2.23
Nb(100)	1.06	1.08	-0.08	-0.14	0.96	1.00	1.84
Ni(111) <sup>a</sup>	0.92	0.94	-0.15	-0.12	1.05	0.98	1.12
Ni(111) <sup>b</sup>	0.93	0.97	-0.08	-0.13	1.04	0.94	1.28
<b>ZrO<sub>2</sub>(110)/</b>							
Ni(110)	0.93	0.93	-0.07	-0.12	0.97	1.03	2.15
Cu(110)	0.98	0.98	-0.07	-0.10	1.01	1.00	1.43
Ni(001)	0.95	0.97	-0.08	-0.18	0.99	0.98	0.94
Cu(001)	1.04	1.05	-0.09	-0.16	1.02	0.95	0.71
<b>HfO<sub>2</sub>/Ni</b>							
(110)/(110)	0.93	0.93	-0.04	-0.09	0.98	1.01	2.09
(111) <sub>O</sub> /(111)	0.94	0.97	-0.05	-0.09	0.96	0.93	1.29
(110)/(001)	0.96	0.98	-0.04	-0.15	1.00	0.98	1.07
<b>MgO/Ag</b>							
(110)/(110)	0.86	0.86	-0.05	-0.12	0.96	1.04	1.10
(100)/(100)	0.99	0.99	-0.04	-0.06	0.94	1.03	0.72
<b>MgO/Na</b>							
(110)/(110)	1.10	1.10	-0.09	0.14	1.01	1.08	0.65
(100)/(100)	1.16	1.16	-0.04	0.20	0.97	1.04	0.17

<sup>a</sup>Aligned with in-plane directions ZrO<sub>2</sub>[1-10]/Ni[1-10] (Ref. 61).

<sup>b</sup>Aligned with in-plane directions ZrO<sub>2</sub>[1-34]/Ni[0-44] (Ref. 62).

TABLE V. Same as Tables III and IV for the interfaces with more than 10% mismatch between a metal overlayer and ZrO<sub>2</sub>.

NST ceramic	$\Delta d$	$\langle \Delta d \rangle$	$\Delta Q_{\text{CER}}$	$\Delta Q_{\text{MET}}$	$\Delta A_{\text{CER}}$	$\Delta A_{\text{MET}}$	Wsep
<b>ZrO<sub>2</sub>(100)<sub>O</sub>/</b>							
Ta(100)	0.97	1.02	-0.07	-0.63	0.97	1.16	10.88
W(100)	1.03	1.08	-0.06	-0.67	0.91	1.19	9.61
Mo(100)	1.03	1.05	-0.10	-0.50	0.96	1.26	9.08
Nb(100)	0.99	1.05	-0.14	-0.49	0.97	1.17	9.07
Rh(100)	0.85	0.86	-0.25	-0.22	1.05	0.93	4.57
Pd(100)	0.88	0.89	-0.27	-0.17	1.06	0.88	2.91
<b>ZrO<sub>2</sub>(111)<sub>O</sub>/</b>							
W(100)	1.01	1.10	-0.05	-0.24	0.92	1.03	2.28
Mo(100)	1.02	1.08	-0.06	-0.19	0.92	1.04	1.85
Cu(111)	0.97	1.03	-0.17	-0.11	1.07	0.94	0.62
<b>ZrO<sub>2</sub>(110)/</b>							
Rh(100)	0.92	0.93	-0.15	-0.11	1.05	1.31	1.94
Pt(100)	0.91	0.92	-0.18	-0.08	1.13	1.31	1.59
Pd(100)	0.98	0.99	-0.10	-0.05	1.00	1.16	0.50

explicitly deduced from the tables such as the metallic character of the interfaces or the rapid decay of the interface effects, characteristics also observed for the adsorption of single metal atoms and layers studied by other authors.<sup>63</sup> Another common feature is the ionic nature of the metal-oxygen bonds, which in all cases involve O charge depletions with respect to the bulk oxide.<sup>7</sup> Although certain ionic character may be assigned to the metal-cation bonds, because of their different electronegativity, the bonds are mainly formed by hybridization of the electronic states and thus in general the electronic bond charge is shared by both metals.

The work of separation cannot be universally correlated with the average interface Mulliken charge due to the diversity on the number of bonds per unit area and the various metal-O and metal-metal pair coordination numbers present at the different interfaces. Even more, bonds with ionic or metallic character show different electronic charge distributions and consequently a different variation in the Mulliken charge. Nevertheless, for a fixed oxide interface the correlation is clear and in general large electron transfer from the metal to the oxygen atoms or large charge shared in the metal-cation bonds corresponds to large  $W_{sep}$ . The fluctuations are due to the coexistence of bonds of different strength in the interface. Therefore, the largest values of  $W_{sep}$  correspond to interfaces with the highest number of strong metal-oxide bonds per unit area, i.e., to the largest charge transfer or largest metal-metal electron hybridization.

The relation between  $W_{sep}$  and the bond lengths is more intricate, partly due to the presence of individual short bond lengths (strong bonds) coexisting with weaker bonds at some interfaces. In general, the strongest interactions correspond to the bcc metals forming interfaces with  $Al_2O_3(0001)$  and  $ZrO_2(001)$ , while the weakest ones are found for MgO both with alkaline and noble metals.

Tables III–V show an important dispersion of  $W_{sep}$  being the difference between the two extreme values larger than an order of magnitude. Nevertheless, these values correspond not only to different metals and different ceramic oxides but also to different lattice orientations which imply variations in lattice structure, polar character of the ceramic surface, and therefore different electronic density distribution. Although the matching of the metal and ceramic structures at the interface has a determinant influence on the adhesion, especially regarding the extended 2D interfaces, some trends for  $W_{sep}$  can also be tracked down concerning the electronic properties. First, for a common number of valence electrons, increasing the metal atomic number ( $Z$ ) enhances  $W_{sep}$ . Second, lower occupancies of the  $d$  band (bcc structures) lead to stronger adhesions, while the adhesion for the Na [ $sp$  valence band (VB)] is very weak. Third, there is a general common property showed by all the interfaces studied; the  $W_{sep}$  for NST oxide surfaces is substantially larger than that corresponding to ST surfaces. In particular, interfaces formed between NST surfaces of oxide ceramics and transition metals of low  $d$ -band occupancy and bcc crystal structure, namely, Nb, Mo, Ta, and W, present a very good adhesion with  $W_{sep}$  of the order of  $10 \text{ J/m}^2$ . On the other side we find that interfaces composed by ST oxide surfaces and metals with high occupancies of the  $d$  band and fcc structure as Cu, Ni, Pd, Pt, Ag, and Rh exhibit much lower  $W_{sep}$ . In fact,

most ST ceramic surfaces correspond to nonpolar terminations except for the  $c\text{-ZrO}_2(111)_O$  and  $c\text{-HfO}_2(111)_O$  polar surfaces ended in a single O-layer, which is a particular case of polar nondivergent surface.<sup>64</sup> For these particular cases, although there is an alternation of positively and negatively charged planes so that the charge at the topmost surface plane is not compensated, the entire ceramic slab has the proper stoichiometry; so these surfaces are stable similarly to the nonpolar ones.

## V. COMPARISON WITH PREVIOUS EXPERIMENTAL RESULTS

In the following, we will compare our results with previous theoretical and experimental works considering each ceramic oxide separately.

Much of the early work on metal/zirconia adhesion was based on the study of the wetting phenomena and the energetics of the interfaces described by the contact angle  $\theta$ . The work of adhesion ( $W_{adh}$ ) and the contact angle are related through the surface energy of the liquid metal,  $\sigma_L$ , by the Young-Dupré equation,  $W_{adh} = \sigma_L[1 + \cos(\theta)]$  (see Ref. 65). The exact value of  $W_{adh}$  that corresponds to wetting experiments is generally lower than that obtained by *ab initio* studies due to the geometry differences as explained in Ref. 65. Nevertheless, for a given oxide the relative trends of variation can be compared. Wettability experiments with different metal melts,<sup>17</sup> using  $ZrO_2$  single crystals as substrate, find a different wetting behavior when comparing ST and NST  $ZrO_2$  substrates. The measured  $\theta$  ranges from  $65^\circ$  to  $150^\circ$  for ST  $ZrO_2$ , while for NST it is reduced from  $60^\circ$  to  $130^\circ$ . The contact angle reduction in NST  $ZrO_2$  indicates that the adhesion is stronger, as we have also obtained (see Tables III–V).

Although *ab initio* studies of the ceramic/metal interface adhesion are quite recent, which implies that in general there are not many results, by far the most studied systems have been those involving  $\alpha\text{-Al}_2O_3$  and Nb, Ni, and Al as metals. For them, an important number of theoretical calculations and experimental works can be found in the literature. Theoretical calculations performed on the  $Al_2O_3(0001)_O/Nb(111)$  interface<sup>9</sup> show the formation of a strong interface with a  $W_{sep}$  of  $9.8 \text{ J/m}^2$  when cleaving the  $Al_2O_3$  at the O plane and of  $2.7 \text{ J/m}^2$  when cleaving at the Al one. This result compares nicely with our value of  $9.3 \text{ J/m}^2$  for the O termination, as well as with the close values that we obtain for the bcc metals Mo, W, and Ta with similar electronic structure than Nb.

Finally, concerning MgO, we have performed calculations only for Na and Ag with similar lattice parameter than that of the ceramic. Ag has been largely studied by *ab initio* calculations, with special emphasis on the effect of the different interface positions on the value of  $W_{sep}$ , as shown in Table VI.

We can see that our calculated  $W_{sep}$  is lower than those obtained previously, but it is the closest to the experimental  $W_{sep}$ . Previous theoretical work<sup>71</sup> has found that alkali metals, and particularly 0.5 and 0.25 ML of Na deposited on MgO (001) show a weak physisorption with higher interaction at the O on-top site than at the Mg site. We obtain

TABLE VI. Values of  $W_{\text{sep}}$  ( $\text{J}/\text{m}^2$ ) for MgO/Ag depending on the relative interface position of the Ag compared to previous calculations (Refs. 66–69) and experimental measurements (Ref. 70).

References	On-top Mg	On-top O
Li	0.54	
Schönberger	0.70	1.60
Heifets	0.63	0.81
Hong	1.08	1.90
Ours	0.27	0.72
Experiment		0.45

similar results with the values of 0.65 and 0.17  $\text{J}/\text{m}^2$  for Na on top of O and Mg, respectively, which in addition are among the lowest  $W_{\text{sep}}$  values for all the systems studied here. From wetting measurements<sup>72</sup> and references therein, the wetting angles for all nonreactive MgO/metal interfaces are over  $90^\circ$ , therefore indicating the low interaction at the interface.

In summary, the calculated values of  $W_{\text{sep}}$  in Tables III–V show a reasonable quantitative agreement with the available experimental and theoretical data.

## VI. WORK OF SEPARATION VS METAL PROPERTIES

If we restrict to a particular ceramic oxide structure,  $c\text{-ZrO}_2$  and  $c\text{-HfO}_2$ , additional dependences of  $W_{\text{sep}}$  on the structural and electronic properties of the metal can be found.

We have studied the correlation between the interface  $W_{\text{sep}}$  and the corresponding strain in the metal slabs. When considering separately NST and ST, the  $W_{\text{sep}}$  is qualitatively well approximated by a linear function of the metal strain. In Fig. 3 the approximate linear dependence is shown for both the ST and NST and  $\text{ZrO}_2$  and  $\text{HfO}_2$  interfaces.  $\text{ZrO}_2$  and  $\text{HfO}_2$  have not only similar electronic configurations but also analogous crystal structures with close lattice parameters.<sup>54</sup> The ST interfaces not only present smaller values of  $W_{\text{sep}}$  than the NST ones but also their variations are smaller for a similar distortion of the 2D metal area. In general, from Fig. 3 it can be concluded that the  $W_{\text{sep}}$  is larger for interfaces with the metal under tensile strain. We have also analyzed

TABLE VII. Bonding overlap population (BOP) for the bulk structures of bcc and fcc metals of Tables III–V ordered by atomic numbers. The total charge for all the metals has been normalized to 1. See Ref. 17 for pseudopotential generation details.

fcc	BOP	bcc	BOP
Ni	0.107	Na	0.350
Cu	0.093	Nb	0.198
Rh	0.120	Mo	0.189
Pd	0.078	Ta	0.201
Ag	0.082	W	0.199
Pt	0.084		

the dependence of  $W_{\text{sep}}$  on the ratio between the bulk 2D unit cells of the metal and the ceramic. We obtain that the larger values of  $W_{\text{sep}}$  are found when the metal area is smaller than that of the ceramic, which again directly relates a high  $W_{\text{sep}}$  with a high metal tensile strain. Since the strain in the metal is tensile, a bond stretching in the metal layer induces an interface bond strengthening and thus increases the interface cohesion.

### Hybridization character and structure

Another correlation may be established between the  $W_{\text{sep}}$  and the electronic properties of the metal. In a solid the total charge of an atom can be decomposed into the Mulliken population and the bonding overlap populations.<sup>73</sup> While the former provides information on the electronic charge balance at each atomic site, the second may be viewed as the amount of charge shared in the bonds. Although both quantities are dependent on the choice of the basis set, they correctly give trends on the amount of charge transfer or the atomic hybridization as long as calculations are performed within a consistent scheme and are sufficiently accurate. Our calculations fulfill both criteria, allowing us to analyze the relation between the calculated  $W_{\text{sep}}$  and the metal bond overlap population (BOP).

Table VII provides the bulk metal BOP for the metals forming the calculated interfaces. Due to the localized nature of the  $d$  band, metals with a  $sp$  VB have larger BOP than

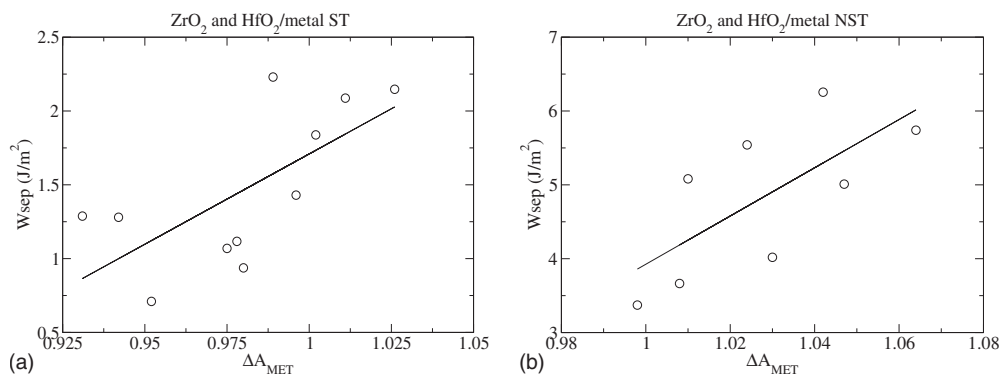


FIG. 3. Relation between the values of  $W_{\text{sep}}$  and  $\Delta A_{\text{MET}}$  for the ST and NST interfaces formed by  $\text{ZrO}_2$  and  $\text{HfO}_2$  with different metals. The continuous lines correspond to a linear fit of the data. Notice the scale of the vertical axis on the right is twice smaller.



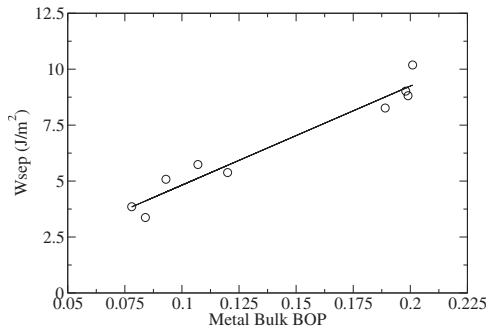


FIG. 4.  $W_{\text{sep}}$  versus the bulk metal BOP for the NST  $\text{ZrO}_2(001)_\text{O}$  interfaces with different (001) metal structures, empty and full circles correspond to fcc and bcc structures, respectively.

those corresponding to metals with a VB formed mainly by  $d$  electrons. Even more, for larger number of  $d$  electrons the BOPs are smaller; then higher hybridization is shown for bcc than for fcc metals. On the other hand, the screening effects tend to increase the BOP with  $Z$  for a fixed number of  $d$  electrons, with the exceptions of Ni and Cu. This must be due to the fact that they are generated with the electronic configurations  $4s^13d^9$  and  $4s^13d^{10}$ , respectively (see Ref. 17 for details in the pseudopotential generation). Figure 4 illustrates the dependence of the  $W_{\text{sep}}$  on the metal BOP for polar  $\text{ZrO}_2(001)_\text{O}/\text{metal}(001)$  interfaces. As previously stated, there is a large difference, around a factor of 2, between the  $W_{\text{sep}}$  for bcc and fcc metals. What Fig. 4 shows is that this large  $W_{\text{sep}}$  correlates with the larger values of the BOP for bcc metals, that is, with the available amount of charge shared in the metal bonds. In a first approximation the correlation can be considered as linear. Moreover, an analysis of the ionic character of the interface metal-O bonds indicates that most of the charge transfer originates from the interstitial metal bond charge.

Also, a relation between large metal BOP values and large  $W_{\text{sep}}$  is found for different ceramics and crystal orientations, as is the case of  $\text{Al}_2\text{O}_3(0001)_\text{O}$ . In general, this relation is valid regarding metals with a valence  $d$  band. However, for Na, showing the largest BOP among all metals, the  $W_{\text{sep}}$  at different  $\text{MgO}$  interfaces is lower than the corresponding value for Ag, with a significantly smaller BOP. On the other hand, the much slighter variations in the BOP when increasing  $Z$  for a fixed number of VB  $d$  electrons can also be correlated with the enhancement of  $W_{\text{sep}}$ .

## VII. WORK OF SEPARATION VS SURFACE AND INTERFACE ENERGIES

As explained in the theoretical methodology, the ideal work of separation can be expressed in terms of the surface and interface free energies [see Eq. (1)].

Thus, the work of separation not only depends on the interface bonds but also on the properties of the surfaces involved. In fact, there is a correlation between  $W_{\text{sep}}$  and  $\sigma$ . We find that interfaces built from surfaces with large  $\sigma$  have larger  $W_{\text{sep}}$  than those containing surfaces with small  $\sigma$ . Figure 5 shows the  $W_{\text{sep}}$  as a function of the sum of the

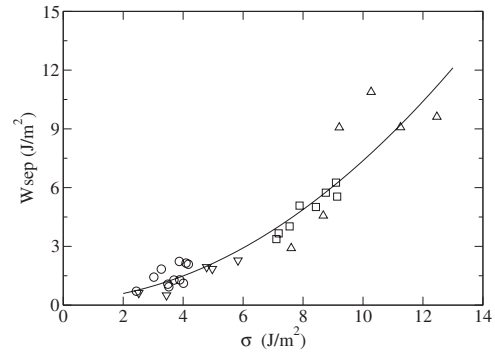


FIG. 5.  $W_{\text{sep}}$  vs  $\langle\sigma\rangle = \langle\sigma_{\text{MET}}\rangle + \langle\sigma_{M_xO_y}\rangle$  for all calculated interfaces. The continuous line represents a quadratic fit to the data, circles (triangles down) corresponds to ST interfaces with misfit of less (more) than 10%, and squares (triangles up) to NST interfaces with misfit of less (more) than 10%.

ceramic and metal surface energies,  $\sigma = \sigma_{\text{MET}} + \sigma_{M_xO_y}$ , for all the calculated interfaces. For polar surfaces,  $\sigma_{M_xO_y}$  is taken as the mean value  $\langle\sigma_{M_xO_y}\rangle$  within the range of allowed  $\mu_\text{O}$  (see Sec. II). Accurate surface energies can only be obtained from calculations with ST ceramic slabs. However, in order to have identical terminations at both sides of the slab, NST slabs terminated in polar surfaces must be used. In this case  $\sigma_{M_xO_y}$  is given as a function of the oxygen chemical potential  $\mu_\text{O}$ . Nevertheless, due to the similar values of  $\Delta G_{M_xO_y}^f$  for the oxides investigated in the present work, the general trend shown in Fig. 5 is almost unchanged regardless of the use of  $\langle\sigma\rangle$  instead of  $\sigma$ .  $\Delta G_{M_xO_y}^f$  takes the values  $-5.37$ ,  $-5.76$ , and  $-5.79$  eV for  $c\text{-ZrO}_2$ ,  $c\text{-HfO}_2$ , and  $\alpha\text{-Al}_2\text{O}_3$ , respectively.

Despite the great variety of interfaces investigated, the relation between  $W_{\text{sep}}$  and  $\sigma$  is parabolic. Note that in Fig. 5 we are including not only different metals, crystal structures, and interface coordinations but also different ceramics and consequently different bonding mechanisms, for example, charge transfer in O-metal bonds or hybridization in cation-metal interactions. A similar trend has been found from a systematic study of Al interfaces with  $\text{Al}_2\text{O}_3$ , nitrides, and carbides.<sup>16</sup>

Furthermore, from Fig. 5 it is evident that interfaces containing oxide polar surfaces with large  $\sigma$  and whose rupture requires the breaking of strong anion-cation ionic bonds present larger  $W_{\text{sep}}$  than those containing nonpolar surfaces. In fact, the formation of interface bonds, and consequently the modification of the surface charge, seems to be a reliable mechanism to decrease the  $\sigma$  and stabilizes polar surfaces, as indicated in their large reactivity.

If we restrict to  $\text{HfO}_2$  and  $\text{ZrO}_2$  (for which we have calculated the largest number of interfaces) and to result from NST slabs (an accurate comparison with ST slabs would require the precise knowledge of  $\mu_\text{O}$ ) the relation is linear, as shown in Fig. 6. Thus, Figs. 5 and 6 suggest that the summed surface energies of the oxide and the metal are the dominant terms in Eq. (1).

However, the interfacial energy  $\gamma$  contribution to  $W_{\text{sep}}$ , although relatively small, is not negligible as was previously proposed.<sup>16</sup> Figure 7 represents the dependence of  $W_{\text{sep}}$  on  $\frac{\gamma}{\sigma}$ , indicating that there are substantial differences between

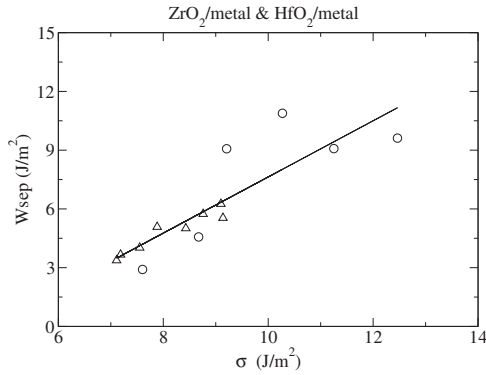


FIG. 6. Same as Fig. 5 for the polar interfaces formed only by HfO<sub>2</sub> or ZrO<sub>2</sub> ceramics. Triangles (circles) correspond to less (more) than 10% misfit between cell constituents.

ST and NST geometries. For ST interfaces  $\gamma$  is comparable to the surface energies,  $\frac{\gamma}{\sigma}$  ranges from 0.4 to almost 0.9, and then the  $W_{sep}$  is not given by the surface energies alone. Nevertheless, for NST interfaces its contribution is not very important, since  $\gamma$  is small in comparison to the surface energies and even may take negative values indicating that interface bonds are as strong as those of the bulk metal and ceramic constituents, thus  $W_{sep} \approx \sigma$ . In particular, NST interfaces formed with bcc metals have the largest  $W_{sep}$ , around 10 J/m<sup>2</sup>, almost independent of the constituents and of the  $\frac{\gamma}{\sigma}$  value.

### VIII. INTERFACE STABILITY

Besides  $W_{sep}$ ,  $\gamma$  gives the excess free energy of an interface compared to the corresponding bulk materials, quantifying the strength of the interfacial bonds with respect to the bulk bonds. In addition, it allows one to know which interfaces are more stable in a thermodynamic sense.  $\gamma$  is calcu-

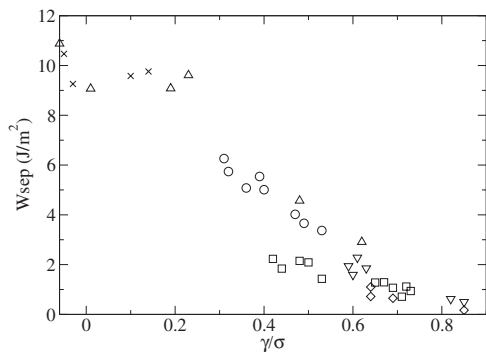


FIG. 7.  $W_{sep}$  vs  $\langle \gamma/\sigma \rangle$  for all calculated interfaces. Crosses correspond to NST interfaces formed by O-terminated Al<sub>2</sub>O<sub>3</sub> and bcc metals with lattice mismatch close to 10%. Inverted triangles correspond to ST ZrO<sub>2</sub>/metal interfaces with more than 10% mismatch. Triangles correspond to NST ZrO<sub>2</sub>(001)/metal interfaces with more than 10% mismatch. NST ZrO<sub>2</sub>(001) and HfO<sub>2</sub>(001) interfaces with fcc metals and less than 10% mismatch are represented by circles. Squares correspond to ST ZrO<sub>2</sub>/metals with less than 10% mismatch. And rhombus indicate ST interfaces constituted by MgO with Ag or Na and mismatch close to 10%.

TABLE VIII.  $\gamma$  for interfaces formed by ST ceramic slabs and the corresponding  $W_{sep}$ , both values are given in J/m<sup>2</sup>.

ST ceramic	$\gamma$	$W_{sep}$
ZrO <sub>2</sub> (111) <sub>O</sub> /Ni(111) <sup>a</sup>	2.89	1.12
HfO <sub>2</sub> (111) <sub>O</sub> /Ni(111)	2.60	1.29
ZrO <sub>2</sub> (110)/Ni(100)	2.59	0.94
HfO <sub>2</sub> (110)/Ni(100)	2.46	1.07
HfO <sub>2</sub> (110)/Ni(110)	2.09	2.09
ZrO <sub>2</sub> (111) <sub>O</sub> /Ni(111) <sup>b</sup>	1.99	1.28
ZrO <sub>2</sub> (110)/Ni(110)	1.95	2.15
ZrO <sub>2</sub> (110)/Cu(100)	1.73	0.71
ZrO <sub>2</sub> (111) <sub>O</sub> /Ta(100)	1.64	2.23
ZrO <sub>2</sub> (110)/Cu(110)	1.59	1.43
ZrO <sub>2</sub> (111) <sub>O</sub> /Nb(100)	1.43	1.84
MgO(110)/Ag(110)	1.99	1.10
MgO(110)/Na(110)	1.42	0.65
MgO(100)/Ag(100)	1.25	0.72
MgO(100)/Na(100)	0.96	0.17

<sup>a</sup>Aligned with in-plane directions ZrO<sub>2</sub>[1–10]/Ni[1–10] (Ref. 61).

<sup>b</sup>Aligned with in-plane directions ZrO<sub>2</sub>[1–34]/Ni[0–44] (Ref. 62).

lated by Eq. (2) as a function of the oxygen chemical potential and therefore of the oxygen pressure.

Table VIII yields the calculated interface energy for the ST interfaces. All the values are positive indicating that the formation of the interface costs energy. The smallest values of  $\gamma$ —those for the most stable interfaces—correspond to MgO even though they also present the smaller  $W_{sep}$ . Similarly to the results obtained for the  $W_{sep}$ , the range of  $\gamma$  are close for the interfaces containing ZrO<sub>2</sub> and MgO, in fact, for the same metal and crystal orientations the interface ZrO<sub>2</sub> and MgO free energies differ by less than 10%. The most stable interface formed by the ZrO<sub>2</sub> and HfO<sub>2</sub> oxides corresponds to *c*-ZrO<sub>2</sub>(111)<sub>O</sub>/Nb(100), which  $W_{sep}$  is also among the largest obtained for ST interfaces. However, the  $\gamma$  variations shown in Table VIII are not very large, indicating that the stabilities of the ST interfaces are analogous.

The calculated  $\gamma$  for the NST interfaces are represented in Tables IX and X, only for the two extreme values of  $\Delta\mu_O$ , 0, and  $\frac{1}{y}\Delta G_{M_xO_y}^f$ , which correspond to high and low oxygen pressures, respectively.  $\gamma$  varies linearly between these two extremes. For  $\Delta\mu_O=0$  ( $\frac{1}{y}\Delta G_{M_xO_y}^f$ ), i.e., high (low) oxygen pressures, the interfaces formed by the anion (cation) termination of the oxide are the most stable. Even more, many interfaces formed by the O-terminated oxides show at high O pressures negative values of  $\gamma$ , which evidences stronger bonds at the interface than those of the bulk structures. Moreover, the Al<sub>2</sub>O<sub>3</sub>/metal interfaces, containing the O-terminated Al<sub>2</sub>O<sub>3</sub> surfaces, present very small  $\gamma$  values at rich O pressures, indicating a rather high stability of these interfaces.

### IX. INTERFACE PROPERTIES BEYOND THE ELASTIC REGIME

The ideal  $W_{sep}$ , defined in Eq. (1), is the reversible work needed to separate the interface into two free surfaces if the

TABLE IX. Interface energies at  $\Delta\mu_O=0$  and  $\Delta\mu_O=\frac{\Delta G_{M_xO_y}^f}{y}$  for NST interfaces formed between fcc metals and ZrO<sub>2</sub> or HfO<sub>2</sub> oxides with less than 10% mismatch and bcc metals with Al<sub>2</sub>O<sub>3</sub>(0001). It also includes the value of the Wsep for each interface and all values are given in J/m<sup>2</sup>. The  $\Delta G^f$  values for *c*-ZrO<sub>2</sub>, *c*-HfO<sub>2</sub>, and  $\alpha$ -Al<sub>2</sub>O<sub>3</sub> is  $-5.37$ ,  $-5.76$ , and  $-5.79$  eV, respectively.

NST ceramic	$\gamma_0$	$\gamma\frac{\Delta G_{M_xO_y}^f}{y}$	Wsep
<hr/>			
Al <sub>2</sub> O <sub>3</sub> (0001) <sub>O</sub> /			
Ta(111)	-3.91	2.91	10.47
W(111)	-1.97	5.06	9.76
Mo(111)	-2.46	4.59	9.58
Nb(111)	-3.65	3.08	9.26
<hr/>			
ZrO <sub>2</sub> (100) <sub>O</sub> /			
Ni(001)	-0.45	5.97	5.74
Cu(001)	-0.37	5.97	5.08
Rh(111)	0.31	6.76	4.02
Pt(111)	0.67	6.81	3.37
<hr/>			
ZrO <sub>2</sub> (100) <sub>Zr</sub> /			
Ni(001)	6.65	0.13	5.01
Cu(001)	6.70	0.35	3.66
<hr/>			
HfO <sub>2</sub> /Ni(001)			
(100)O	-0.43	6.12	6.26
(100)Zr	6.63	0.26	5.54

plastic and diffusional degrees of freedoms are suppressed. Due to the neglect of these terms, Wsep always represents a lower bound for the fracture energy measured in any cleavage experiment.<sup>17,65</sup>

However some insight into the ability to mechanical reinforcement of a particular system can be gained by comparing the adhesion properties at the interface, characterized by Wsep, to those of the constituent materials.

Applying Eq. (1) for homogeneous materials, the work of separation needed to form two surfaces from the bulk structure is given by  $Wsep_i=2\sigma_i$ , where  $\sigma_i$  ( $i=MET, M_xO_y$ )

TABLE X. Same as Table IX for the interfaces formed by fcc and bcc (001) metals with ZrO<sub>2</sub>(001) with more than 10% mismatch.

NST ceramic	$\gamma_0$	$\gamma\frac{\Delta G_{M_xO_y}^f}{y}$	Wsep
<hr/>			
ZrO <sub>2</sub> (100) <sub>O</sub> /			
Ta(100)	-3.97	2.74	10.88
W(100)	-0.68	6.41	9.61
Mo(100)	-1.23	5.51	9.08
Nb(100)	-3.24	3.43	9.07
Rh(100)	1.10	7.26	4.57
Pd(100)	1.65	7.78	2.91

TABLE XI. Wsep and surface energies of the ceramic and metal for NST interfaces with <10% mismatch. The underlined quantity indicates the region (ceramic, metal, or interface) where crack failure is expected to occur. All quantities are given in J/m<sup>2</sup>.

NST ceramic	$2\sigma_{CER}$	$2\sigma_{MET}$	Wsep
<hr/>			
Al <sub>2</sub> O <sub>3</sub> (0001) <sub>O</sub> /			
Ta(111)	13.97	<u>5.97</u>	10.47
W(111)	14.43	<u>8.18</u>	9.76
Mo(111)	14.45	<u>6.84</u>	9.58
Nb(111)	13.78	<u>4.16</u>	9.26
<hr/>			
ZrO <sub>2</sub> (100) <sub>O</sub> /			
Ni(001)	12.04	<u>5.48</u>	5.74
Cu(001)	12.48	<u>3.30</u>	5.08
Rh(111)	10.24	4.86	<u>4.02</u>
Pt(111)	10.80	3.42	<u>3.37</u>
<hr/>			
ZrO <sub>2</sub> (100) <sub>Zr</sub> /			
Ni(001)	11.42	5.44	<u>5.01</u>
Cu(001)	11.16	<u>3.22</u>	3.66
<hr/>			
HfO <sub>2</sub> /Ni(001)			
(100)O	12.80	<u>5.40</u>	6.26
(100)Zr	12.91	<u>5.37</u>	5.54

stands for the surface energy of the material considered, either the metal or the ceramic. Therefore, from the knowledge of  $\sigma_{MET}$ ,  $\sigma_{M_xO_y}$ , and the interface Wsep, it is possible to predict the place of failure of a heterogeneous interface in a cleavage experiment since it fails on the region of weakest bonds.

Tables XI and XII compile the adhesion values for different interfaces and the corresponding metal and oxide surface energies. For the NST ZrO<sub>2</sub> and HfO<sub>2</sub> surfaces (second block), all the Wsep values are higher than the metal surface energies except for ZrO<sub>2</sub>(100)<sub>Zr</sub>/Ni(001), ZrO<sub>2</sub>(100)<sub>O</sub>/Rh(111) and ZrO<sub>2</sub>(100)<sub>O</sub>/Pt(111). On the other hand, all the interfaces formed by the Al<sub>2</sub>O<sub>3</sub> show Wsep values well above those of the metal surface energies. The average surface energy of the oxide is always larger. Therefore, it is expected that NST interfaces will commonly fail in the metal region. Contrarily, for interfaces built from ST surfaces, see Table XII, the Wsep is the smallest quantity but for MgO(110)/Na(110) and ZrO<sub>2</sub>(111)<sub>O</sub>/Ta(100). Therefore, they will fail at the interface, presenting brittle debonding.

We would like to point out that our calculations are valid under the elastic regime, beyond which is expected that the start of the metal plastic deformation contributes further to the reinforcement of the system.<sup>74</sup> In fact, many fracture experiments on  $\alpha$ -Al<sub>2</sub>O<sub>3</sub> and metals such as Nb, Al, Ni, Cu, or Au have shown toughening mechanisms such as the crack blunting, which is based on the plastic deformation of the metal and can induce fracture energies above 200 J/m<sup>2</sup> with no need of a very good interface matching.<sup>5</sup> A summary of the experimental measurements is shown in Ref. 75. Particu-

TABLE XII. Same as Table XI but for ST interfaces. All quantities are given in J/m<sup>2</sup>.

ST ceramic	$2\sigma_{\text{CER}}$	$2\sigma_{\text{MET}}$	Wsep
ZrO <sub>2</sub> (111) <sub>O</sub> /			
Ta(100)	<u>2.02</u>	5.72	2.23
Nb(100)	2.04	4.50	<u>1.84</u>
Ni(111) <sup>a</sup>	3.32	4.70	<u>1.12</u>
Ni(111) <sup>b</sup>	2.46	4.92	<u>1.28</u>
ZrO <sub>2</sub> (110)/			
Ni(110)	2.84	5.36	<u>2.15</u>
Cu(110)	2.66	3.38	<u>1.43</u>
Ni(100)	1.72	5.34	<u>0.94</u>
Cu(100)	1.58	3.30	<u>0.71</u>
HfO <sub>2</sub> /Ni			
(110)/(110)	2.90	5.44	<u>2.09</u>
(111) <sub>O</sub> /(111)	2.74	5.04	<u>1.29</u>
(110)/(100)	1.62	5.36	<u>1.07</u>
MgO/Ag			
(110)/(110)	4.08	2.11	<u>1.10</u>
(100)/(100)	1.74	2.19	<u>0.72</u>
MgO/Na			
(110)/(110)	3.70	<u>0.45</u>	0.65
(100)/(100)	1.78	0.48	<u>0.17</u>

<sup>a</sup>Aligned with in-plane directions ZrO<sub>2</sub>[1–10]/Ni[1–10] (Ref. 61).

<sup>b</sup>Aligned with in-plane directions ZrO<sub>2</sub>[1–34]/Ni[0–44] (Ref. 62).

larly, a reported fracture energy of  $112 \pm 51$  J/m<sup>2</sup> has been found for the Al<sub>2</sub>O<sub>3</sub>(0001)/Nb(111) interface, indicating that a mechanism of plasticity may occur.<sup>76</sup>

The  $\alpha$ -Al<sub>2</sub>O<sub>3</sub>(0001)/Mo(111) interface has also been studied in cermets formed by a polycrystalline ceramic matrix including metal particles.<sup>77</sup> An increase in the fracture energy from 20 to 60 J/m<sup>2</sup> is obtained when the concentration of the metal increases from near 0% to 20%, with a bridging mechanism induced by ductile particles. Our results again compare qualitatively well since we obtain plastic reinforcement in this system. Therefore, although plasticity effects are not taken specifically into account in our calculations, we expect from Tables XI and XII a plastic reinforcement for every bcc metal when forming interfaces with  $\alpha$ -Al<sub>2</sub>O<sub>3</sub>(0001), in agreement with the available experimental measurements.

Furthermore, we consider another criterion of interface failure based on the stress intensity that settles the start of plastic deformation in the metal. The local stress intensity (Kie) needed for the emission of the first dislocation, and therefore the beginning of the plastic regime, has been obtained by a three-dimensional (3D) molecular-dynamics simulation for various fcc metals.<sup>78</sup> The available values for the fcc metals, involved in the interfaces described in Tables

TABLE XIII. Stress intensity ( $K_{\text{IC}}$ ) of the interfaces with <10% of mismatch and formed by fcc metals to compare with the available local stress intensity (Kie) values of the metal (Ref. 78), both values given in MPa  $\sqrt{m}$ .

NST ceramic	$K_{\text{IC}}$	Kie
MxO <sub>2</sub> /Ni(001)		
HfO <sub>2</sub> (100) <sub>O</sub>	1.18	1.10
ZrO <sub>2</sub> (100) <sub>O</sub>	1.11	1.10
HfO <sub>2</sub> (100) <sub>Hf</sub>	1.13	1.10
ZrO <sub>2</sub> (100) <sub>Zr</sub>	1.06	1.10
MxO <sub>2</sub> /Cu(001)		
ZrO <sub>2</sub> (100) <sub>O</sub>	0.86	0.71
ZrO <sub>2</sub> (100) <sub>Zr</sub>	0.73	0.71
ZrO <sub>2</sub> (100) <sub>O</sub> /Pt(111)	0.80	0.63
ST ceramic		
MxO <sub>2</sub> /Ni		
ZrO <sub>2</sub> (110)/(110)	0.69	1.10
HfO <sub>2</sub> (110)/(110)	0.68	1.10
HfO <sub>2</sub> (111) <sub>O</sub> /(111)	0.54	1.10
ZrO <sub>2</sub> (111) <sub>O</sub> /(111) <sup>a</sup>	0.54	1.10
ZrO <sub>2</sub> (111) <sub>O</sub> /(111) <sup>b</sup>	0.50	1.10
HfO <sub>2</sub> (110)/(100)	0.49	1.10
ZrO <sub>2</sub> (110)/(100)	0.46	1.10
MxO <sub>2</sub> /Cu		
ZrO <sub>2</sub> (110)/(110)	0.46	0.71
ZrO <sub>2</sub> (110)/(100)	0.32	0.71

<sup>a</sup>Aligned with in-plane directions ZrO<sub>2</sub>[1–10]/Ni[1–10] (Ref. 61).

<sup>b</sup>Aligned with in-plane directions ZrO<sub>2</sub>[1–34]/Ni[0–44] (Ref. 62).

XI and XII, are given in Table XIII together with the phenomenological stress intensity assigned to the interface ( $K_{\text{IC}}$ ) as derived from our calculated Wsep,<sup>74</sup>

$$K_{\text{IC}} = \sqrt{\frac{W_{\text{sep}} E_{\text{Young}}}{(1 - \nu^2)}},$$

where  $\nu$  is the Poisson modulus and  $E_{\text{Young}}$  is the Young modulus of the constituent metals. The Poisson modulus for polycrystalline metals is fairly constant and close to 0.33, which is the value we employ for all the metals. The value of  $K_{\text{IC}}$  calculated from the metal parameters gives the lowest limit of the interface stress intensity since  $K_{\text{IC}}$  obtained from the oxide parameters is always larger.

If  $K_{\text{IC}} > \text{Kie}$  dislocations are formed at the metal side and the mechanical properties of the complete interface are improved by a toughening mechanism. From the Table XIII we can see that for NST interfaces  $K_{\text{IC}}$  is generally larger than Kie, being both stress intensity values rather similar, while for the ST cases  $K_{\text{IC}}$  is around two times smaller than Kie. These results compare well with those previously obtained in

Tables XI and XII and tell us that an enhancement of the adhesion by the bridging mechanism may occur in almost all NST interfaces.

## X. CONCLUSIONS

A systematic investigation of the adhesion properties of a broad range of oxide/metal interfaces has been performed by *ab initio* DFT methods. General trends of the behavior of  $W_{sep}$ , which characterizes the mechanical properties of the oxide/metal system in the elastic regime as a function of the charge, structure, and strain conditions of the constituent materials are established.

Differences as large as one order of magnitude in the  $W_{sep}$  have been obtained depending on the surface of the oxide. The higher  $W_{sep}$  are found for nonstoichiometric geometries, which mainly correspond to O-terminated oxide polar surfaces. While stoichiometric interfaces, related to nonpolar oxide terminations, present  $W_{sep}$  values substantially smaller than those corresponding to the nonstoichiometric surfaces. Moreover, the crystal structure of the transition metal also influences the  $W_{sep}$  resulting in general in higher values for bcc than for fcc transition metals. Further, the strain conditions affect the interface adhesion and larger values of  $W_{sep}$  are found for strained configurations. The

calculated  $W_{sep}$ 's follow a parabolic dependence on the summed surface energies of the metal and the oxide regardless of the oxide and metal components, crystal lattice, orientations, or atomic terminations. The interfacial energy contribution to  $W_{sep}$ , although non-negligible, is smaller compared to the surface energy contribution, especially for nonstoichiometric geometries which show the largest  $W_{sep}$ .

In addition, an attempt to analyze the nonelastic fracture mechanisms is also accomplished. The comparison of the interface crack resistance and those associated to the metal and oxide bulk allows us to estimate the region of failure of the system and to discuss whether a reinforcement of the mechanical properties by plastic deformation of the metal takes place. Our analysis indicates that interfaces formed by nonstoichiometric oxides are frequently reinforced by plastic mechanisms, while for stoichiometric geometries the oxide/metal interface fails by decohesion and no plasticity reinforcement is obtained.

## ACKNOWLEDGMENTS

We are very grateful to J.F. Bartolomé, S. Gallego, C. Pecharrmán, and J.S. Moya for many fruitful discussions. This work was supported by the Spanish Ministry of Education and Science under Project No. MAT2006-05122.

\*juan.beltran@materianova.be

<sup>1</sup>S. Roberts and R. J. Gorte, *J. Phys. Chem.* **95**, 5600 (1991).

<sup>2</sup>H. Kim, P. C. McIntyre, C. O. Chui, K. C. Saraswat, and S. Stemmer, *J. Appl. Phys.* **96**, 3467 (2004).

<sup>3</sup><http://www.kmm-noe.org/DesktopDefault.aspx?tabindex=75&=219>

<sup>4</sup>B. Lawn, *Fracture of Brittle Solids* (Cambridge University Press, Cambridge, 1993).

<sup>5</sup>A. G. Evans, D. R. Mumm, J. W. Hutchinson, G. H. Meier, and F. S. Pettit, *Prog. Mater. Sci.* **46**, 505 (2001).

<sup>6</sup>J. F. Bartolomé, J. I. Beltrán, C. F. Gutiérrez-González, C. Pecharrmán, M. C. Muñoz, and J. S. Moya, *Acta Mater.* **56**, 3358 (2008).

<sup>7</sup>C. Pecharrmán, J. I. Beltrán, F. Esteban-Betegón S. López-Esteban, J. F. Bartolomé, M. C. Muñoz, and J. S. Moya, *Z. Metallkd.* **96**, 507 (2005).

<sup>8</sup>S. B. Sinnott and E. C. Dickey, *Mater. Sci. Eng., R.* **43**, 1 (2003).

<sup>9</sup>I. G. Batyrev, A. Alavi, and M. W. Finnis, *Phys. Rev. B* **62**, 4698 (2000).

<sup>10</sup>M. Lane, *Annu. Rev. Mater. Res.* **33**, 29 (2003).

<sup>11</sup>A. G. Evans and B. J. Dalgleish, *Mater. Sci. Eng., A* **162**, 1 (1993).

<sup>12</sup>R. Grau-Crespo, N. Cruz Hernández, J. F. Sanz, N. H. de Leeuw, *J. Phys. Chem. C* **111**, 10448 (2007).

<sup>13</sup>M. Alfredsson and C. R. A. Catlow, *Phys. Chem. Chem. Phys.* **4**, 6100 (2002).

<sup>14</sup>W. Zhang, J. R. Smith, and A. G. Evans, *Acta Mater.* **50**, 3803 (2002).

<sup>15</sup>A. Bogicevic and D. R. Jennison, *Phys. Rev. Lett.* **82**, 4050

(1999).

<sup>16</sup>D. J. Siegel, L. G. Hector, Jr., and J. B. Adams, *Phys. Rev. B* **67**, 092105 (2003).

<sup>17</sup>M. C. Muñoz, S. Gallego, J. I. Beltrán, and J. Cerdá, *Surf. Sci. Rep.* **61**, 303 (2006).

<sup>18</sup>J. I. Beltrán, S. Gallego, J. Cerdá, J. S. Moya, and M. C. Muñoz, *Phys. Rev. B* **68**, 075401 (2003).

<sup>19</sup>J. I. Beltrán, S. Gallego, J. Cerdá, J. S. Moya, and M. C. Muñoz, *J. Phys. Chem. B* **108**, 15439 (2004).

<sup>20</sup>J. M. Soler, E. Artacho, J. D. Gale, A. Garcia, J. Junquera, P. Ordejón, and D. Sánchez-Portal, *J. Phys.: Condens. Matter* **14**, 2745 (2002).

<sup>21</sup>P. Hohenberg and W. Kohn, *Phys. Rev.* **136**, B864 (1964).

<sup>22</sup>W. Koch and M. C. Holthausen, *A Chemist's Guide to Density Functional Theory* (WCH-Wiley, Weinheim, 2001).

<sup>23</sup>J. P. Perdew, K. Burke, and M. Ernzerhof, *Phys. Rev. Lett.* **77**, 3865 (1996).

<sup>24</sup>H. J. Monkhorst and J. D. Pack, *Phys. Rev. B* **13**, 5188 (1976).

<sup>25</sup>V. N. Staroverov, G. E. Scuseria, J. Tao, and J. P. Perdew, *Phys. Rev. B* **69**, 075102 (2004).

<sup>26</sup>J. H. Cho and M. Scheffler, *Phys. Rev. B* **53**, 10685 (1996).

<sup>27</sup><http://www.webelements.com/>.

<sup>28</sup>S. Curtarolo, D. Morgan, and G. Ceder, *Calphad* **29**, 163 (2005).

<sup>29</sup>J. C. Bailor, H. J. Emeleus, R. S. Nyholm, and A. F. Trotman-Dickenson, *Comprehensive Inorganic Chemistry* (Pergamon Press, Oxford, 1973).

<sup>30</sup>E. Wachowicz and A. Kiejna, *J. Phys.: Condens. Matter* **13**, 10767 (2001).

<sup>31</sup>F. Willaime, *J. Nucl. Mater.* **323**, 205 (2003).

<sup>32</sup>A. S. Foster, F. Lopez Gejo, A. L. Shluger, and R. M. Nieminen,

- Phys. Rev. B **65**, 174117 (2002).
- <sup>33</sup>J. Malcolm W. Chase, Jr., *NIST-JANAF Thermochemical Tables, Fourth Edition, J. Phys. Chem. Ref. Data*, Monograph 9 (1998).
- <sup>34</sup>D. J. Siegel, Ph.D. thesis, University of Illinois, 2001.
- <sup>35</sup>W. Y. Ching and Y.-N. Xu, *J. Am. Ceram. Soc.* **77**, 404 (1994).
- <sup>36</sup>*CRC Handbook of Chemistry and Physics*, 67th ed., edited by R. C. Weast (CRC, Boca Raton, FL, 1983).
- <sup>37</sup>P. Richet, J. Xu, and H. K. Mao, *Phys. Chem. Miner.* **16**, 207 (1988).
- <sup>38</sup>H. d'Amour, D. Schiferl, W. Denner, H. Schulz, and W. B. Holzapfel, *J. Appl. Phys.* **49**, 4411 (1978).
- <sup>39</sup>G. Geneste, J. Morillo, and F. Finocchi, *Appl. Surf. Sci.* **188**, 122 (2002).
- <sup>40</sup>A. R. Oganov and P. I. Dorogokupets, *Phys. Rev. B* **67**, 224110 (2003).
- <sup>41</sup>J. Kang, E.-C. Lee, and K. J. Chang, *Phys. Rev. B* **68**, 054106 (2003).
- <sup>42</sup>I. M. Iskandarova, A. A. Knizhnik, E. A. Rykova, A. A. Bagatur'yants, B. V. Potapkin, and A. A. Korkin, *Microelectron. Eng.* **69**, 587 (2003).
- <sup>43</sup>J. E. Lowther, J. K. Dewhurst, J. M. Leger, and J. Haines, *Phys. Rev. B* **60**, 14485 (1999).
- <sup>44</sup>N. I. Mednedeva, V. P. Zhukov, M. Y. Khodos, and V. A. Gubanov, *Phys. Status Solidi B* **160**, 517 (1990).
- <sup>45</sup>G. Jomard, T. Petit, A. Pasturel, L. Magaud, G. Kresse, and J. Hafner, *Phys. Rev. B* **59**, 4044 (1999).
- <sup>46</sup>A. S. Foster, V. B. Sulimov, F. Lopez Gejo, A. L. Shluger, and R. M. Nieminen, *Phys. Rev. B* **64**, 224108 (2001).
- <sup>47</sup>L. K. Dash, N. Vast, P. Baranek, M.-C. Cheynet, and L. Reining, *Phys. Rev. B* **70**, 245116 (2004).
- <sup>48</sup>S. Fabris, A. T. Paxton, and M. W. Finnis, *Phys. Rev. B* **61**, 6617 (2000).
- <sup>49</sup>E. V. Stefanovich, A. L. Shluger, and C. R. A. Catlow, *Phys. Rev. B* **49**, 11560 (1994).
- <sup>50</sup>P. Aldebert and J.-P. Traverse, *J. Am. Ceram. Soc.* **68**, 34 (1985).
- <sup>51</sup>C. J. Howard, R. J. Hill, and B. E. Reichert, *Acta Crystallogr. B* **B44**, 116 (1988).
- <sup>52</sup>R. J. Ackermann, E. G. Rauh, and C. A. Alexander, *High. Temp. Sci.* **7**, 304 (1975).
- <sup>53</sup>R. P. Ingel and D. Lewis III, *J. Am. Ceram. Soc.* **71**, 265 (1988).
- <sup>54</sup>V. Fiorentini and G. Gulleri, *Phys. Rev. Lett.* **89**, 266101 (2002).
- <sup>55</sup>N. Sanchez, S. Gallego, and M. C. Muñoz (unpublished).
- <sup>56</sup>I. G. Batyrev, A. Alavi, and M. W. Finnis, *Phys. Rev. B* **62**, 4698 (2000).
- <sup>57</sup>K. Reuter and M. Scheffler, *Phys. Rev. B* **65**, 035406 (2001).
- <sup>58</sup>J. I. Beltrán, Ph.D. thesis, University Auton Madrid, 2007.
- <sup>59</sup>J. I. Beltrán, M. C. Muñoz, and J. Hafner, *New J. Phys.* **10**, 063031 (2008).
- <sup>60</sup>J. I. Beltrán, S. Gallego, J. Cerdá, and M. C. Muñoz, *J. Eur. Ceram. Soc.* **23**, 2737 (2003).
- <sup>61</sup>T. Sasaki, K. Matsunaga, H. Ohta, H. Hosono, T. Yamamoto, and Y. Ikuhara, *Mater. Trans.* **45**, 2137 (2004).
- <sup>62</sup>A. Christensen and E. A. Carter, *J. Chem. Phys.* **114**, 5816 (2001).
- <sup>63</sup>A. Eichler and G. Kresse, *Phys. Rev. B* **69**, 045402 (2004).
- <sup>64</sup>P. W. Tasker, *J. Phys. C* **12**, 4977 (1979).
- <sup>65</sup>M. W. Finnis, *J. Phys.: Condens. Matter* **8**, 5811 (1996).
- <sup>66</sup>C. Li, R. Wu, A. J. Freeman, and C. L. Fu, *Phys. Rev. B* **48**, 8317 (1993).
- <sup>67</sup>U. Schönberger, O. K. Andersen, and M. Methfessel, *Acta Metall. Mater.* **40**, S1 (1992).
- <sup>68</sup>E. Heifets, R. Orlando, R. Dovesi, C. Pisani, and E. A. Kotomin, *Second International Conference on Computer Simulation Radiation Effects in Solids* (Santa Barbara, 1994).
- <sup>69</sup>T. Hong, J. R. Smith, and D. J. Srolovitz, *J. Adhes. Sci. Technol.* **8**, 837 (1994).
- <sup>70</sup>A. Trampert, F. Ernst, C. P. Flynn, H. F. Fischmeister, and M. Rühle, *Acta Metall. Mater.* **40**, S227 (1992).
- <sup>71</sup>J. A. Snyder, J. E. Jaffe, M. Gutowski, Z. Lin, and A. C. Hess, *J. Chem. Phys.* **112**, 3014 (2000).
- <sup>72</sup>N. Eustathopoulos and B. Drevet, *Mater. Sci. Eng., A* **249**, 176 (1998).
- <sup>73</sup>R. Hoffmann, *Solids and Surfaces: A Chemist's View of Bonding in Extended Structures* (VCH-Wiley, New York, 1988).
- <sup>74</sup>J. E. Reynolds, J. R. Smith, G.-L. Zhao, and D. J. Srolovitz, *Phys. Rev. B* **53**, 13883 (1996).
- <sup>75</sup>A. G. Evans, J. W. Hutchinson, and Y. Wei, *Acta Mater.* **47**, 4093 (1999).
- <sup>76</sup>G. Soyez, G. Elssner, M. Rühle, and R. Raj, *Acta Mater.* **46**, 3571 (1998).
- <sup>77</sup>O. Sbaizero, G. Pezzotti, and T. Nishida, *Acta Mater.* **46**, 681 (1998).
- <sup>78</sup>J. Knap and K. Sieradzki, *Phys. Rev. Lett.* **82**, 1700 (1999).